Macromolecular Bioscience
www.mbs-journal.de

Photoinduced Amyloid Fibril Degradation for Controlled Cell Patterning

Kübra Kaygisiz, Adriana M. Ender, Jasmina Gačanin, L. Alix Kaczmarek, Dimitrios A. Koutsouras, Abin N. Nalakath, Pia Winterwerber, Franz J. Mayer, Hans-Joachim Räder, Tomasz Marszalek, Paul W. M. Blom, Christopher V. Synatschke, and Tanja Weil**

Amyloid-like fibrils are a special class of self-assembling peptides that emerge as a promising nanomaterial with rich bioactivity for applications such as cell adhesion and growth. Unlike the extracellular matrix, the intrinsically stable amyloid-like fibrils do not respond nor adapt to stimuli of their natural environment. Here, a self-assembling motif (CKFKFQF), in which a photosensitive *o*-nitrobenzyl linker (PCL) is inserted, is designed. This peptide (CKFK-PCL-FQF) assembles into amyloid-like fibrils comparable to the unsubstituted CKFKFQF and reveals a strong response to UV-light. After UV irradiation, the secondary structure of the fibrils, fibril morphology, and bioactivity are lost. Thus, coating surfaces with the pre-formed fibrils and exposing them to UV-light through a photomask generate well-defined areas with patterns of intact and destroyed fibrillar morphology. The unexposed, fibril-coated surface areas retain their ability to support cell adhesion in culture, in contrast to the light-exposed regions, where the cell-supportive fibril morphology is destroyed. Consequently, the photoresponsive peptide nanofibrils provide a facile and efficient way of cell patterning, exemplarily demonstrated for A549, Chinese Hamster Ovary, and Raw Dual type cells. This study introduces photoresponsive amyloid-like fibrils as adaptive functional materials to precisely arrange cells on surfaces.

1. Introduction

Nature creates function through complex self-organization processes. In the past few decades, great progress has been made in mimicking these ordered nanostructures with synthetic biomaterials.[1] To mimic natural cell distribution and study cell migration and communication, the spatial control of cell-attachment (cell patterning) is of great interest.[2–4] The most frequently used approaches for cell-patterning focus on controlling the stiffness and texture of substrates or the position of cell attractive molecules on inorganic substrates or biomaterials.[2,5–8] However, these methods usually lack spatiotemporal control of the morphology of the cellular environment, which plays an essential part in natural matrices that are constantly reshaped by various stimuli.[9] For instance, directed cell alignment is controlled by patterning of fibrillar structures from self-assembling peptides (SAPs).[10] These fibrillar morphologies have crucial functions in living cells; and are thus, highly prevalent in the extracellular matrix to enhance material–cell interactions to support proliferation and cell infiltration at the mesoscopic length scale.[11–13]

Amyloid fibrils are a subclass of SAPs and nature's intrinsically bioactive nanofibrils. They are characterized by their high cross β-sheet content, mechanical stiffness, stability toward enzymatic degradation, and strong adhesion to various substrates.[14] The best known are amyloid structures in misfolded proteins that lead to insoluble plaques associated with several neurodegenerative diseases.[15–17] However, naturally occurring amyloids fulfill various purposes in organisms as scaffold materials.[18,19] For example, they are involved in the formation of bacteria biofilms[20,21] or as scaffolds for hormone storage[22] and melanin polymerization.[23] Recently, the potential of amyloid nanostructures serving in beneficial roles has been exploited in 3D cell culture, gene delivery, tissue, and neuronal regeneration, as well as in drug delivery.[24–26] This is due to the cell adhesive properties that were found for some artificial amyloid fibrils. However, because of the inherent stability of the amyloid fibrils, they cannot readily be quantitatively disassembled in a short time,[27] which would be a prerequisite to study morphology dependent

K. Kaygisiz, A. M. Ender, J. Gačanin, L. A. Kaczmarek, P. Winterwerber, F. J. Mayer, H.-J. Räder, C. V. Synatschke, T. Weil
Department Synthesis of Macromolecules
Max Planck Institute for Polymer Research
Ackermannweg 10, 55128 Mainz, Germany
E-mail: synatschke@mpip-mainz.mpg.de; tweil@mpip-mainz.mpg.de
D. A. Koutsouras, A. N. Nalakath, T. Marszalek, P. W. M. Blom
Department of Molecular Electronics
Max Planck Institute for Polymer Research
Ackermannweg 10, 55128 Mainz, Germany
T. Marszalek
Department of Molecular Physics
Faculty of Chemistry
Lodz University of Technology
Zeromskiego 116, Lodz 90-924, Poland

The ORCID identification number(s) for the author(s) of this article can be found under https://doi.org/10.1002/mabi.202200294

DOI: 10.1002/mabi.202200294

cell-adhesive properties, for example, for the application as adaptive scaffold biomaterials. Synthetic amyloid-like short SAPs that spontaneously form β-sheet-rich nanofibrils through noncovalent interactions[25,28] are not related to amyloids found in neurodegenerative diseases and exhibit several distinctively different features. They can be chemically customized to design next generation functional biomaterials with controllable stability and bioactivity.[17,29,30]

To gain control over the formation of amyloid structures and thereby their bioactivities, several groups have established strategies to disassemble already formed fibrils. Changing environmental parameters such as peptide concentration and pH can lead to disassembly as these parameters affect the equilibrium of fibril formation.[31] Furthermore, additives such as ruthenium(II)-complexes,[32] fullerenes,[33] water–ethanol mixtures,[34] amphiphilic polyphenylene dendrimers,[35] PEG-chains,[36] carbon nanotubes,[37] and molecular chaperons[38,39] have been applied to disassemble amyloid fibrils. However, these methods cannot be applied for controlled spatiotemporal modification after fibrils are embedded in complex environments. Instead, stimulus-sensitive reactive groups have been incorporated in the peptide sequence to initiate morphological changes of fibrils.[40] For example, azobenzene and hydrazone groups that undergo a *cis–trans* isomerization after irradiation[41–43] or depsipeptides that reveal a pH-induced structural transition from a kinked to a linear structure[44,45] have been proposed to control peptide assembly and disassembly. In these instances, highest spatiotemporal control can only be achieved with light. Since the first pioneering works on photoresponsive manipulation of the cell environment,[46–49] a variety of spatial cell-patterning techniques have been applied.[50] The overwhelming amount of reports modulates cell attachment by introducing or removing bioactive molecules[51–54] or locally changing stiffness of the polymeric (bio)material by crosslinking or bond scission.[55–57] Photoresponsive approaches for modulating structural changes in self-assembly of peptides are rarely reported[58] and not applied for cell-patterning. *o*-Nitrobenzyl ester is a well-established photoresponsive molecule and can be combined with peptides to attach bioactive molecules.[11,59] For example, using this photocleavable linker (PCL) attached to amyloid-like fibrils, we previously created functional cell-gradients by photocleavage of a bioactive moiety from the fibrillar backbone.[60] It is important to note that in these published reports, the fibrillar backbone of the nanofibrils remained intact and also cell-adherent to some extent, limiting the generation of unique cell patterns.

In this work, we solve this limitation by introducing the PCL cleavage motif into the backbone of an amphiphilic SAP sequence. UV-irradiation fully destroys the amyloid-like fibrillar morphology, resulting in a complete loss of bioactivity. Consequently, cell-patterning is achieved by coating the fibrils on surfaces and irradiating them with UV-light through a photomask. Our strategy demonstrates a direct connection between amyloid morphology and bioactivity, which is exploited to study cell attachment and migration in artificial cell-matrices. We envision that the spatiotemporal control over structural integrity gives access to tailored and customizable 4D cell-culture.

2. Results and Discussion

2.1. Design, Synthesis, and Characterization of the Photoresponsive Self-Assembling Peptide

The peptide sequence CKFKFQF assembles into cell-adhesive nanofibrils in aqueous media (Figure S1, Supporting Information) and was used as scaffold for the design of photocleavable nanofibrils that provide the capacity to disintegrate upon irradiation. CKFKFQF forms biocompatible amyloid-like structures, which were previously shown to enhance neuronal outgrowth in vitro.[61] We hypothesized that the bioactivity can be traced back to the fibril morphology and speculated that changes in sequence length or amphiphilicity will affect the assembly and bioactivity for short sequences such as CKFKFQF. Furthermore, due to its amphiphilic sequence composed of hydrophobic, non-charged phenylalanine (F) and hydrophilic, cationic Lysine (K) amino acids, this peptide represents an ideal starting point to study the effect on assembly by cleaving the hydrophilic charged peptide part from the lipophilic part. In our concept, a PCL was implemented between the third (F) and fourth (K) amino acid of this sequence, resulting in CKFK-PCL-FQF 1. Even after integration of the PCL linker, this sequence formed amyloid-like nanofibrils serving as bioactive scaffold and stimulating cell adhesion and growth. UV irradiation leads to a molecular scission of PCL, resulting in the disintegration of the nanofibrils and the formation of fragments 2 and 3 (**Figure 1**A), which cannot form fibrils (Figure S1, Supporting Information). In addition, the non-photoreactive control peptide CKFK-NCL-FQF (4, Scheme S1, Supporting Information) was synthesized and characterized (Figures S8 and S9, Supporting Information).

Peptide synthesis of 1 and 4 was conducted via solid phase peptide synthesis (Scheme S1, Supporting Information) using Wang resin. The PCL as well as NCL linkers were synthesized and conjugated to the solid phase bound peptides as described previously.[60] Purification of the peptides was accomplished applying reversed-phase high performance liquid chromatography (rp-HPLC). Successful synthesis and purity (>95%) were validated by matrix-assisted laser desorption/ionization time-of-flight mass spectrometry (MALDI-ToF-MS) and liquid chromatography mass spectrometry (LC-MS), respectively (Figure 1B; Figure S2, Supporting Information). Next, the photocleavage kinetics were determined by time-dependent measurements, in which aliquots of 1 (1 mg mL^{-1} in water) were analyzed by HPLC starting with a non-irradiated sample and irradiation times of up to 20 min (Figure 1C). Using LC-MS measurements (Figure S3, Supporting Information), the signal with the retention time of 10.2 min was assigned to the intact peptide showing a mass-to-charge ratio (m/z) of 1285.70, matching the protonated $[1+H]^+$ adduct. After 10 min UV treatment at 365 nm, less than 10% of the intact peptide was detected (Figure 1D). An additional kinetic study was performed, by incubating 1 in dimethylsulfoxide (DMSO). After 1 min of UV-irradiation, complete photocleavage of the peptide CKFK-PCL-FQF was observed (Figure S4, Supporting Information), indicating that the cleavage kinetics strongly depend on the selected solvent.[62] In contrast, UV-irradiation of the non-cleavable control peptide CKFK-NCL-FQF did not alter its structure nor its elution time after 10 min of

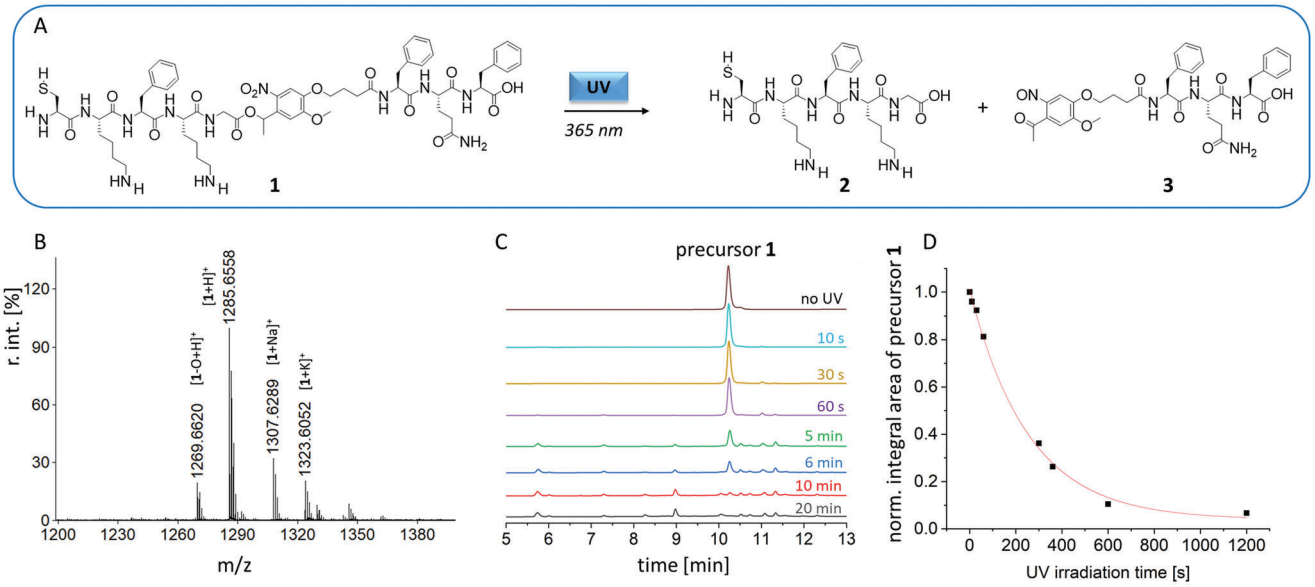

Figure 1. A) Scheme of molecular cleavage of the designed peptide CKFK-PCL-FQF 1 under UV-irradiation. B) MALDI-ToF-MS spectra of the purified peptide CKFK-PCL-FQF, 1, MS calcd. for $[1+H]^+$, 1285.59 g mol $^{-1}$; found m/z 1285.66, calcd for $[1+Na]^+$, 1307.57 g mol^{-1}; found 1307.63 m/z, calcd. for $[1\text{-}O+H]^+$, 1269.60 g mol^{-1} found m/z 1269.66. The loss of oxygen ascribed with the mass 1269.66 $[1\text{-}O+H]^+$ is caused by high laser power of the MALDI-ToF-MS measurement in HCCA matrix.[75] C) HPLC spectra of CKFK-PCL-FQF peptide after different UV-irradiation times in aqueous solution. After 10 min irradiation, the precursor molecule 1 is completely cleaved. Several decomposition products of 1 are detected via LC-MS (Figure S3, Supporting Information). Absorbance detected at 254 nm. D) First-order kinetics of the integral area from LC traces of the precursor molecule 1 at t_{Ret} 10.2 min normalized to 1 without irradiation (no UV).

irradiation in water (Figures S10–S12, Supporting Information) or DMSO (Figure S1, Supporting Information).

2.2. Secondary Structure and Morphology of Amyloid-Like Fibrils Are Altered After Irradiation

We designed CKFK-PCL-FQF to form amyloid-like fibrils in water at pH 7.4 with similar morphology (**Figure 2**E) as the original bioactive peptide sequence CKFKFQF (Figure S1, Supporting Information).[63] The only difference in the structure is the PCL linker, which serves as cleavage site for controlled linker degradation (Figure 2A). After UV irradiation of the CKFK-PCL-FQF nanofibrils, the β-sheet secondary structure was lost, as evidenced by the decrease of the characteristic cotton peaks for β-sheet structure[64] elements at 196 and 222 nm in circular dichroism (CD) measurements (Figure 2B).

The photoinduced cleavage and disintegration of the β-sheet structures were further supported by attenuated total reflectance fourier transform infrared (ATR-FTIR) spectroscopy measurements of lyophilized peptides (Figure 2C). Here, the non-irradiated fibrils showed absorbance maxima in the amide I region at 1630 and 1664 cm^{-1} corresponding to β-sheet and β-turn structures, respectively, as well as absorbance in the amide II region at ≈1520 cm^{-1}, corresponding to β-sheet structures.[65] Upon irradiation of the fibrils in solution, the peak at 1630 cm^{-1} in the amide I region disappeared, whereas the peak at 1664 cm^{-1} increased and the amide II band at 1520 cm^{-1} decreased compared to the non-irradiated sample. These experimental results indicated loss of β-sheet structures and increase of non-ordered and α-helical structural elements.[44,66]

To elucidate whether the β-sheet structures of the fibrils dispersed in aqueous media, the Thioflavin-T (ThT) assay was conducted, which indicates the presence of amyloid structures by an increase in fluorescence intensity of the ThT molecule after binding to ordered β-sheets structures.[67] In this assay, fluorescence intensity of ThT decreased after irradiation of CKFK-PCL-FQF fibrils (Figure 2D), revealing the reduction of β-sheet-rich amyloid-like structures. Interestingly, the ThT fluorescence further decreased, when incubating the irradiated sample in solution for 72 h. This was in contrast to the non-irradiated sample, which showed no decrease in ThT-fluorescence after 72 h. The time-dependent decrease in ThT-fluorescence indicates a hysteretic degradation of irradiated fibrils. Transmission electron microscopy (TEM) images that were recorded directly after irradiation for 20 min (Figure 2E) revealed fragments of broken fibrils, which further transformed to irregular aggregates during the selected observation time of 72 h (Figure S5, Supporting Information). Fragments of broken fibrils may retain the ability to bind ThT to a certain extent whereas the irregular aggregates cannot. Obviously, the supramolecular structures were destabilized over a prolonged period of time whereas the intermolecular changes altering the packing of the peptide monomers within the nanofibrils already occurred during the irradiation process.

Liquid-mode atomic force microscopy (liquid-AFM) measurements of in situ irradiated nanofibrils allowed us to directly study the fragmentation of the nanofibril during irradiation. A clear transition from elongated nanofibrils into spherical aggregates (Figure 2F) was observed. The degradation of the fibrillar morphology was also supported by turbidity measurements of the fibril solution, which increased directly after

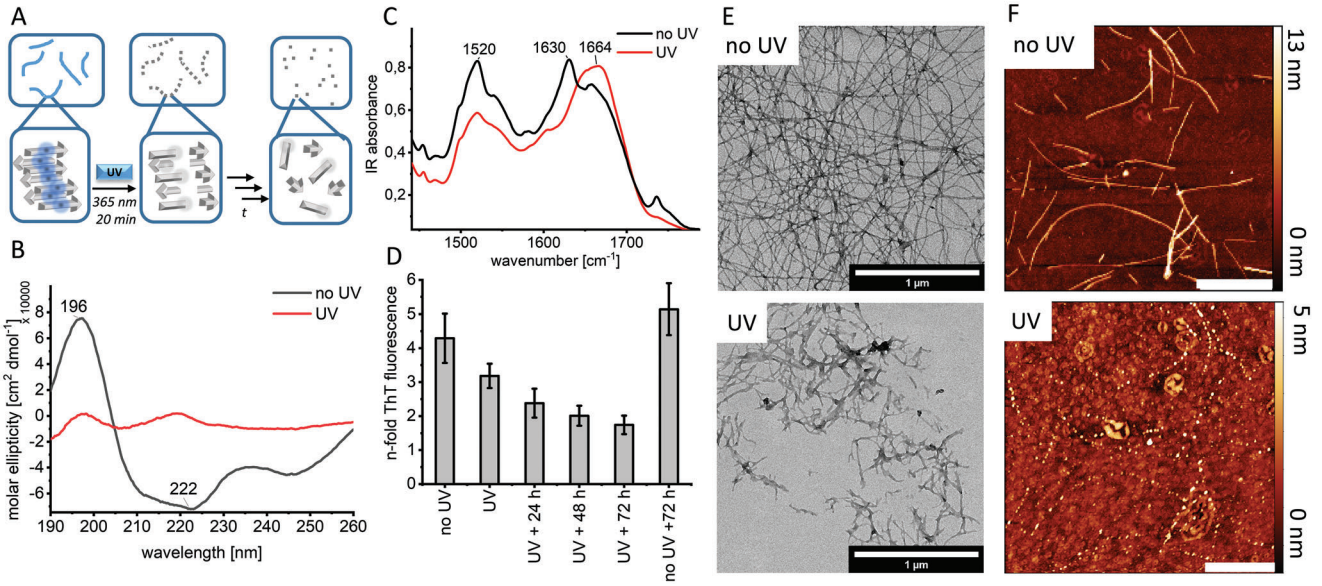

Figure 2. Secondary structure and morphology of CKFK-PCL-FQF fibrils before and after UV irradiation for 20 min. A) Schematic illustration of photocleavage of the peptide sequence upon irradiation, which destabilizes the amyloid-like fibrils. B) CD spectra of non-irradiated versus irradiated fibrils reveal loss of secondary structure after irradiation. C) ATR-FTIR spectra of non-irradiated and irradiated fibril samples indicate loss of β-sheet structures in the amide I and II regions. D) Thioflavin-T Assay of non-irradiated fibrils as well as fibrils irradiated for 20 min at 365 nm and incubated at room temperature for 24, 48, and 72 h. The bar plot shows the n-fold fluorescence relative to ThT fluorescence in water at pH 7.4, excitation 440/10 nm, and emission 488/10 nm. E) TEM micrographs of fibrils before (top) and after irradiation (bottom) displaying morphological changes, scalebar: 1 µm. F) Liquid AFM measurements of the fibrils (top) after in situ irradiation for 20 min (bottom) showing destabilization of fibrils into fragments, scalebar: 500 nm.

irradiation and further over the following three days. We interpreted the increased turbidity by the formation of a large number of aggregates of the newly formed peptide fragments, indicated by enhanced light scattering of the dispersed sample (Figure S6, Supporting Information). The degradation of the nanofibrils did not result in a complete disassembly and solvation of the peptide as shown by microscopy measurements (Figure S5, Supporting Information) and by a conversion assay which quantifies aggregated monomers (Figure S7, Supporting Information).[63] We traced the aggregated structures back to the peptide fragment 3, which is highly lipophilic due to the phenylalanine side chain residues and the *N*-terminal nitrosobenzyl group. Noteworthy, these aggregated peptide fragments did not have β-sheet secondary order as shown by CD and FTIR (Figure 2B,C).

In contrast, the integrity of the control peptide CKFK-NCL-FQF was not affected by photoirradiation (TEM, Figure S11, Supporting Information; AFM, Figure S12, Supporting Information; and ThT-assay, Figure S13, Supporting Information), confirming that the observed structural changes of CKFK-PCL-FQF were due to the photoinduced bond cleavage of the PCL. Photoirradiation of the CKFK-PCL-FQF nanofibrils therefore resulted in immediate loss of the β-sheet structures because of the scission of the peptide backbone in a cationic, hydrophilic (CKFK), and lipophilic (FQF) part. The resulting destabilization of the intermolecular interactions between peptide monomers further led to fragmentation of the fibrillar assembly into aggregates with no β-sheet secondary order.

2.3. Photopatterning of Fibril-Coated Surfaces

Next, we investigated whether photolithography could be used to create defined patterns of intact and degraded amyloid-like nanofibrils to create distinct cell-adhesive regions on substrates (**Figure 3**A). Initially, optical microscope glass slides were covered with a thin agarose layer[60] using a dip coating technique. The agarose layer of ≈50 nm thickness (Figure S14, Supporting Information) shows a cell-repellent character and is applied to suppress nonspecific cell adhesion.[61,68–70] Subsequently, the slides were coated with an amyloid-like fibril layer via drop casting. As agarose forms gels by physical crosslinks via hydrogen bonds, these interactions may also stabilize the attachment of the peptide fibrils coating and agarose layer.[71–73] A photolithography mask was used to cover parts of the peptide film, leaving the rest of it exposed to UV-light. Thereby, a pattern of choice can be imbued on the substrate that was previously coated with CKFK-PCL-FQF.

We applied different photomasks with different resolution for the photopatterning of peptide nanofibrils (Figure S15, Supporting Information). We established mass spectrometry imaging (MALDI-MSI) for characterizing the identity of the formed fragments on the surface. MALDI-MSI directly determines the chemical species on the surface and reveals the distribution of the fragmented peptide **2** with a spatial resolution up to 100 µm (Figure S17, Supporting Information). Moreover, photopatterning was visually demonstrated by the Proteostat assay that only stains intact amyloid structures, which can then be detected by fluorescence microscopy. The surface areas that were directly exposed to

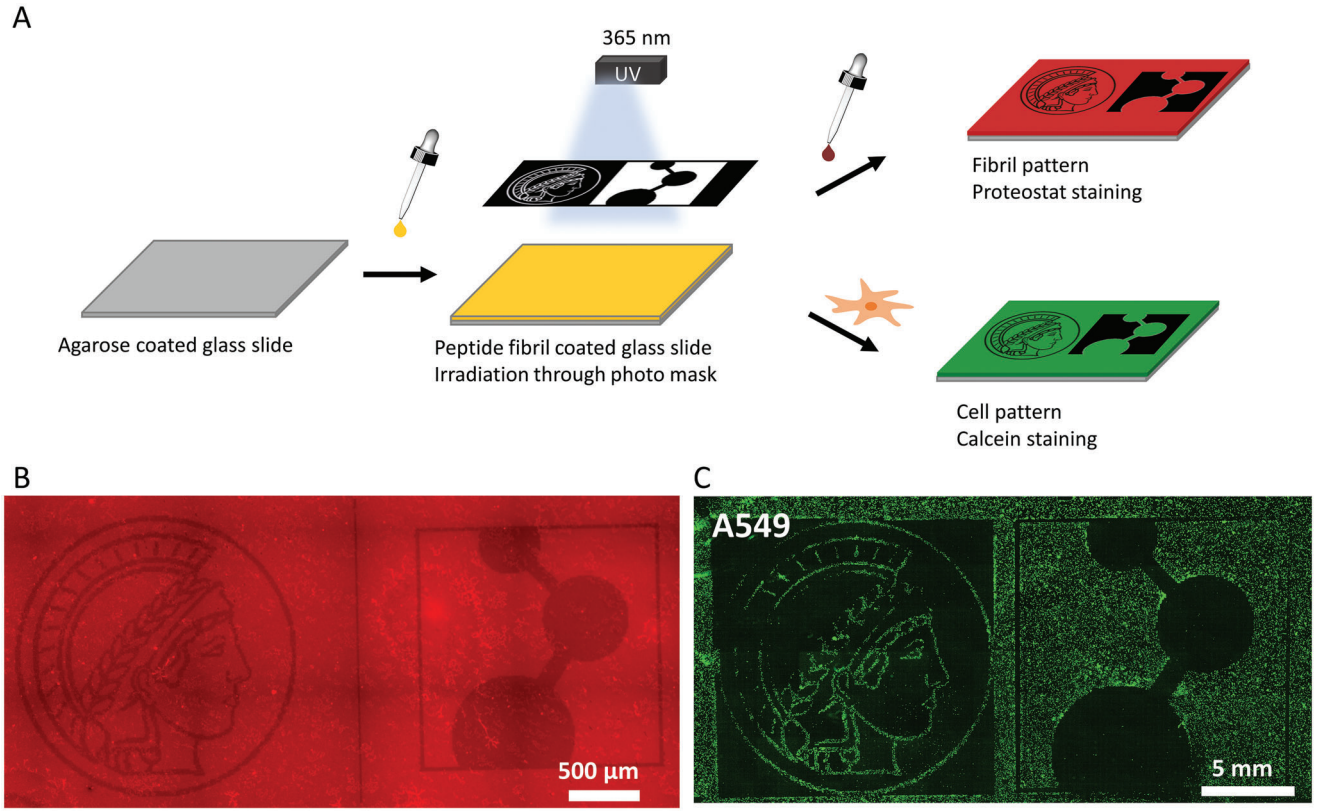

Figure 3. Patterning of glass slides coated with photocleavable amyloid-like fibrils. A) Schematic representation of the workflow. The peptide layer is applied on an agarose pre-treated glass slide and exposed to UV-light through a photomask. The fibril morphology is destroyed where UV-light can reach the surface, which is visualized via fluorescence microscopy of Proteostat-stained samples. Before seeding the cells, the photopatterned surface is stored for 5 h in water to allow morphology change of the irradiated parts. Cells seeded for 15 h on the patterns only attach to the non-irradiated regions, where fibrils remain intact. B) Fluorescence microscope image of Proteostat-stained photopatterned peptide layer depicting the head of Minerva and MPIP logo (scalebar: 500 µm). C) Fluorescence microscopy image of A549 cells seeded on photopatterned peptide layer. The UV exposure alters the ability of the amyloid-like fibrils to sustain cell culturing and results in cell patterning (scalebar: 5 mm).

UV-light reveal less fluorescence and appear darker compared to the non-exposed regions. Via this photopatterning technique, resolutions down to 10 µm could be achieved (Figure 3B; Figure S16, Supporting Information), which is in the size-range of a single A549 cell and thereby suitable for accurate cell patterning.

2.4. Spatially Controlled Cell Pattern

We have reported previously that bioactive amyloid-like nanofibrils, which bind to cellular membranes[63] and support neuronal outgrowth,[61] require a positive net charge, fibrillar morphology, as well as high content of β-sheet structures. As demonstrated in the previous sections, the intact CKFK-PCL-FQF peptide can provide these features in regard to their morphology (Figure 2) and charge (Figure S22, Supporting Information) but loses them upon irradiation. We therefore aimed to create spatial cell patterns by photoinduced degradation of these fibril properties and applied A549, Chinese Hamster Ovary (CHO), and Raw-Dual type cells as model cell-lines. The cell distribution was analyzed by fluorescence microscopy and attached viable cells were stained in green with calcein (Figure S18, Supporting Information). The CellTiter-Glo assay confirmed the non-toxic character of irradiated and non-irradiated fibril regions (Figure S19, Supporting Information). A549 cells (Figure 3C), CHO, and Raw-Dual cells (Figure S20, Supporting Information) did not attach to irradiated areas whereas non-irradiated areas with intact fibril-coating showed robust cell attachment which was due to differences in morphology and secondary structure of irradiated and non-irradiated fibril areas. Control experiments without peptide coating and with the non-photoresponsive CKFK-NCL-FQF fibrils did not show any cell attachment and cell patterning, respectively (Figure S21, Supporting Information). To determine the resolution limit for cell-patterning, we applied a photomask with elements of different size down to 10 µm (Figure S15B, Supporting Information **Figure 4**A). Cell patterns could be clearly identified for fibril patterned elements larger than 100 µm (Figure 4B-i,ii). Motifs smaller than 40 µm (Figure 4B-iii,C-iii) could not be resolved. In summary, cell patterning was achieved by photopatterning of photocleavable peptides on surfaces. Intact fibrillar morphology induced cellular attachment whereas photocleavage of irradiated fibril surface areas resulted in complete loss of their ability to support cell adhesion.

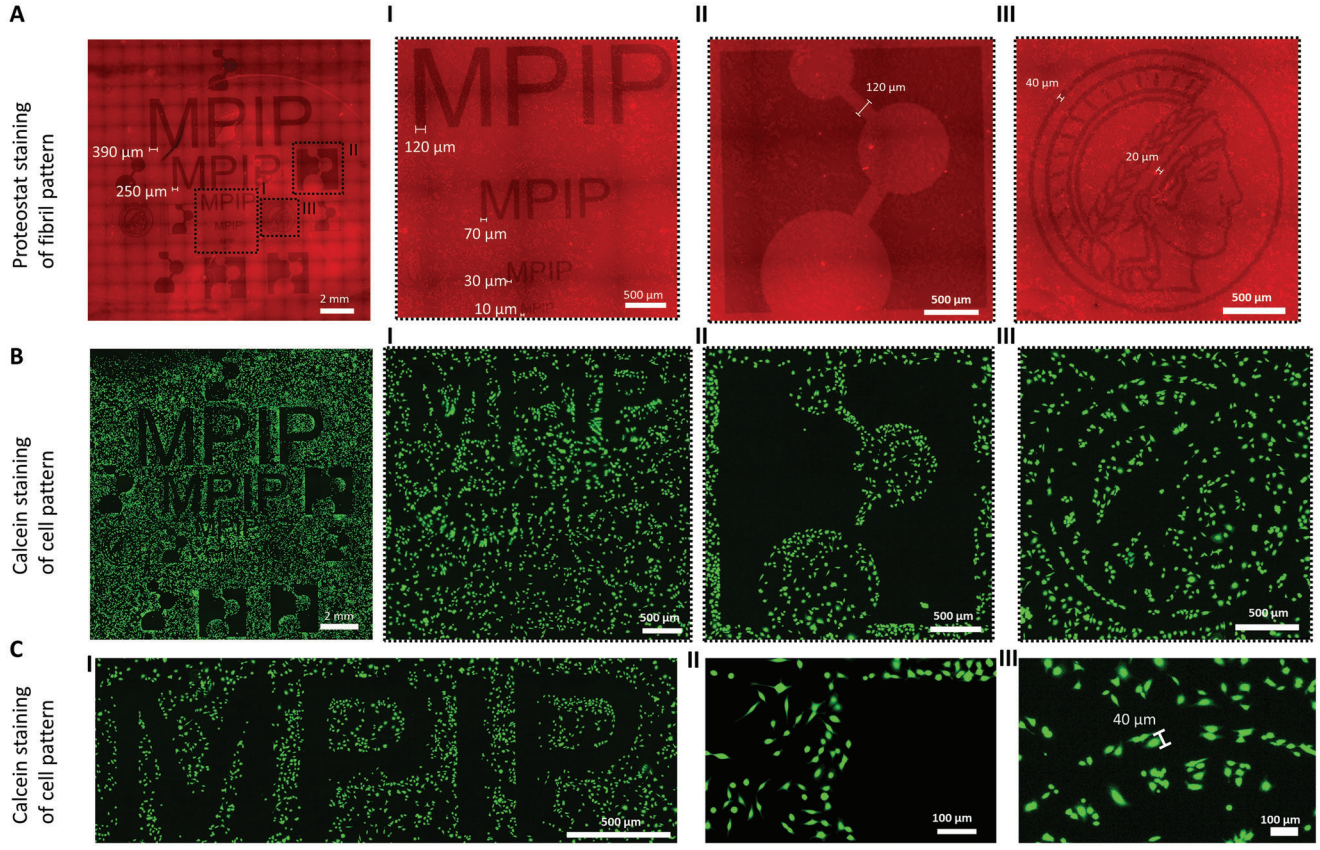

Figure 4. Cell pattern resolution limit shown for A549 cells, which were incubated on a photopatterned peptide fibril surface. A) The photomask (Figure S15B, Supporting Information) enables the creation of motifs of various sizes as shown via Proteostat staining (scalebar: 2 mm). A-i–iii) shows regions of interest depicting the smallest resolvable motif, which is 10 µm as part of the letter "M" (scalebar: 500 µm). B) Cells seeded on this photopatterned surface (B, scalebar: 2 mm) show that cell pattern can be clearly observed for motifs with a size larger than 100 µm (B-i-iii, scalebar: 500 µm) but not for motifs smaller than 40 µm (B-iii, scalebar: 500 µm). C) Enlarged details of B-i-iii) (C-i; scalebar: 500 µm), (C-ii,iii; scalebar: 100 µm) show cell alignment at the borders of the patterning motifs. Distance bars show width of indicated patterning elements.

3. Conclusion

We have successfully demonstrated the synthesis of a photoreactive SAP sequence that forms cell-adhesive fibrillar surface coatings supporting spatially controlled cell attachment. Positioning the PCL at a critical position within the self-assembling sequence resulted, after the irradiation process, in the formation of a positively charged and a lipophilic fragment that were no longer able to form ordered, cell-adhesive nanofibrils. Fibril morphology was locally destroyed through UV-light irradiation as an external trigger resulting in immediate loss of β-sheet structures, nanofibril morphology, and cell adhesiveness of the SAPs. Using photomasks, cell-adhesive and cell-repulsive areas were fabricated with resolutions of up to 10 µm precision. We envision that this method could be applied to create UV-treatable peptide layers on various substrates and various cell-types to realize a versatile cell patterning technique and establish amyloid-like fibrils as adaptive functional materials in biologically relevant model environments. Embedding these photoresponsive peptide fibrils into a 3D cell-matrix for spatiotemporal control over structural integrity may provide access to tailored and customizable 4D cell culture materials. More broadly, these findings are important beyond biomaterials applications by providing a direct correlation between morphology and cell-interactions and for understanding bioactivity of amyloid fibrils in general.

4. Experimental Section

Materials: For peptide synthesis, OxymaPure, Fmoc-Cys(Trt)-OH, Fmoc-Gln(Trt)-OH, Fmoc-Gly-OH, Boc-Gly-OH, and Fmoc-Phe-Wang resin, and (2-(1*H*-benzotriazol-1yl)-1,1,3,3-tetramethyluronium hexafluorophosphate (HBTU) were purchased from Novabiochem, Merck. Fmoc-Lys(Boc)-OH, Fmoc-Phe-OH, piperidine, trifluoroacetic acid (TFA), *N,N*-di*iso*propylethylamine (DIPEA), and *N,N″*-diisopropylcarbodiimide were purchased from Carl Roth GmbH + Co. KG. Peptide-synthesis-grade solvents (dichloromethane and dimethylformamide) were acquired from Acros Organics. Solvents used for synthesis were purchased in HPLC grade purity or higher from Sigma–Aldrich (diethyl ether, DMSO, ethanol), Fisher Scientific (dichloromethane, chloroform, hexane, dimethylformamide, acetone, acetonitrile, ethyl acetate, and tetrahydrofuran), or VWR Chemicals (methanol). Proteostat was purchased from Enzo Life Sciences. Thioflavin-T was purchased from Sigma–Aldrich. Dulbecco's modified eagle medium (DMEM), F-12K Nutrient Mixture Kaighns's Modification (Nut Mix (1X)), heat-inactivated (30 min at 56 °C) fetal bovine serum (FBS), MEM non-essential amino acid solution, penicillin (10.000 U per mL), and streptomycin (10 000 µg mL^{-1}) were purchased from Gibco (Darmstadt, Germany). Normocin and Zeocin were purchased from InvivoGen.

Methods: *Linker-Synthesis*: The photocleavable (PCL, 4-(4-(1-(([(9*H*-fluoren-9-ylmethoxy)carbony]glycyl)oxy)ethyl)-2-methoxy-5-nitrophenoxy) butanoic acid) and non-photocleavable (NCL, 4-(4-(2-(2-([(9*H*-fluoren-9-ylmethoxy)carbonyl]amino)acetamido)ethyl) phenoxy)butanoic acid) linkers were synthesized according to literature.[11,60]

Solid-Phase Peptide Synthesis and Characterization of CKFK-PCL-FQF 1 and CKFK-NCL-FQF 4: Peptides were synthesized using an automated microwave peptide synthesizer (CEM, Liberty BlueTM) from *C* to *N*-terminus according to fluorenylmethyloxycarbonyl (Fmoc) solid phase peptide synthesis strategy by Merrifield using the Fmoc-L-Phe-Wang resin (Scheme S1, Supporting Information). The coupling reaction of the PCL[60] (5 equiv.) or NCL[60] (5 equiv.) to the peptide sequence FQF on solid phase was performed manually in DMF with HBTU (5 equiv.) and DIPEA (10 equiv.) for 24 h at room temperature. Successive coupling of the following amino acids (CKFK) was carried out using an automated microwave peptide synthesizer as described in detail in Section S1.1, Supporting Information. Cleavage from the resin was performed by shaking in a solution of TFA containing 2.5% water and 2.5% tri*iso*propylsilane for 2 h at room temperature. This solution was added to cold diethyl ether (40 mL) to afford a white precipitate and afterward centrifuged three times at 4 °C, 4000 rpm for 15 min. The precipitate was dissolved in water with 0.1% TFA and purified via high performance liquid chromatography (HPLC) (Shimadzu modules DGU-20A5R, LC-20AP, CBM-20A, SPD-M20A, SIL-10AP, and FRC-18A with Phenomenex Gemini 5 µm NX-C18, 110 Å, 150 × 30 mm) using a gradient of water and acetonitrile containing 0.1% TFA as the mobile phase at a flow rate of 25 mL min^{-1}. Chromatography was monitored with a UV absorption detector at 214 and 254 nm. After lyophilization, a white solid (yield 10%) was obtained. The peptides were identified via matrix assisted laser desorption/ionization time of flight (MALDI-ToF) mass spectrometry and purity (>95%) was confirmed by LC-MS. MALDI-ToF-MS was conducted on a Bruker rapifleX MALDI-TOF/TOF and a Waters MALDI Synapt G2-SI instrument. The samples were mixed with a saturated α-cyano-4-hydroxycinnamic acid (HCCA) solution in water/ACN 1:1 + 0.1% TFA before measurement and applied to the target via dried droplet method.[74] The data were evaluated with mMass software. LC-MS was conducted on a Shimadzu LC-2020 Single Quadrupole MS instrument with the modules LC-20AD, SIL-20ACHT, SPD-20A, and CTO-using a Kinetex EVO and C18 100 Å LC 50 × 2.1 mm column with 2.6 µm pore size. A gradient of acetonitrile/water mixture with 0.1% formic acid (5% ACN to 95% ACN over 20 min) was used as eluent. Samples were dissolved either in methanol or MilliQ water to a concentration of 0.01 mg mL^{-1} and monitored at 214 nm absorption. The data were processed with LabSolutions and Origin.

Photocleavage Kinetics in Solution: The photocleavage kinetics in solution were conducted analogous to a previous report.[60] Briefly, the peptides were predissolved in DMSO to a concentration of 10 mg mL^{-1} and subsequently diluted to a concentration of 1 mg mL^{-1} with pure MilliQ water. Irradiation was conducted using an LED by Opulent Americas (Starboard Luminus SST-10-UV-A130, $\lambda = 365$ nm) operating at a current of 1 A and a radiant flux of 875 mW with varying exposure times ranging from 0 to 20 min. 50 µL of the samples was injected per run in a Shimadzu system (modules DGU-20A5R, LC-20AT, CBM-20A, SPD-M20A, SIL-10ACHT, and CTO-20AC) with an Agilent ZORBAX Eclipse XDB-C18, 80 Å, 5 µm, 9.4 × 250 mm column at a flow rate of 4 mL min^{-1} and MilliQ water and ACN with 0.1% TFA as a gradual eluent from 5% to 80% ACN in 15 min.

Nanofibril-Formation: The peptides were predissolved in DMSO to a concentration of 10 mg mL^{-1}. The solution was immediately diluted to 1 mg mL^{-1} using MilliQ water. The pH was adjusted to 7.4 ± 0.4 using 0.1 M NaOH and 0.1 M HCl solutions and checked with a pH electrode. To complete fibril formation, the pH-adjusted peptide solution was incubated 24 h at room temperature.

Amyloid-Like Fibril Characterization From Solution: Transmission electron microscopy (TEM) measurements, ThioflavinT (ThT) measurements, and attenuated total reflection Fourier transform infrared (ATR-FTIR) spectra for nanofibril characterization were prepared and conducted analogous to a previous report.[60] Monomer to fibril conversion was determined as previously reported.[63] CD measurements were conducted on a JASCO 1500 instrument in a 1 mm quartz cuvette (HellmaAnalytics) from 190 to 260 nm with preformed fibrils diluted to 0.1 mg mL^{-1}. For the characterization of irradiated samples, the preformed fibrils were irradiated in solution with an LED by Opulent Americas (Starboard Luminus SST-10-UV-A130) operated at 365 nm at a current of 1 A and a radiant flux of 875 mW. Unless indicated otherwise, the characterization was conducted immediately after irradiation. The characterization of irradiated fibrils was conducted analogous to non-irradiated samples.

Precoating of Microscope Slides With Agarose: Glass slides were precleaned with acetone and *iso*propanol. An aqueous agarose solution (1 wt%) was cooked 1 h in order to obtain a fully dissolved and transparent solution. The slides were then dipped in the hot (90 °C) agarose solution for 3 min and thereafter slowly (800 µm $s-^{1}$) lifted up from the solution with an automated stage. The slides were air-dried before further usage.

Fabrication of Nanofibril-Coated Surfaces: Surface coatings of SAPs were achieved by homogenous distribution and incubation of 300 µL, 0.25 mg mL^{-1} preformed fibrils on agarose-coated microscopy slides (75 by 26 mm) overnight. Excess solvent was removed by flipping and the slides were dried. After photo-patterning, the slides were stored in MilliQ for 5 h before conducting cell studies.

Irradiation of Surface With Photomask: In order to create patterns of irradiated photoresponsive SAP, a photolithography mask (SELBA) was applied. UV exposure was realized with an LED by Opulent Americas (Starboard Luminus SST-10-UV-A130, 20 min, $\lambda = 365$ nm, 1 A, 875 mW) for the patterning of motifs (Figure S15A, Supporting Information) or with a SÜSS MicroTec MA6 mask aligner (10 s, $\lambda = 365$ nm, 9 mW cm^{-2} 350 W Hg) for the photopatterning of motif (Figure S15B, Supporting Information).

Atomic Force Microscopy: Atomic force microscopy (AFM) was conducted in liquid state with a JPK NW III atomic force microscope for compound 1 or with a Bruker Dimension FastScan BioTM atomic force microscope for compound 4. AFM probes with a nominal force constant of 2 N m^{-1} or 0.25 N m^{-1} were used, respectively and operated in tapping mode with a resonance frequency of 70 kHz (OLTESPA-R3, Bruker). Samples were irradiated in situ by using an LED by Opulent Americas (Starboard Luminus SST-10-UV-A130) operating at a current of 1 A, 875 mW at 365 nm for 20 min while being measured. Images were processed with Gwyddion 2.59.

Pattern Analysis by Proteostat Assay: Proteostat-staining was applied as an amyloid-sensitive dye to detect intact fibrils after UV treatment of 1. A Proteostat Kit by Enzo Lifesciences was used for analysis. 1 µL of the assay buffer was diluted in 99 µL MilliQ water. 0.1 µL of the Proteostat stock solution was added and thoroughly mixed and 500 µL of the solution was placed on the sample to cover the peptide-coated area as well as a part of the non-coated area for reference. After incubation in the dark for 15 min, the solution was removed and samples were dried. The measurement was conducted on a Leica Thunder DMI8 microscope coupled to a Leica DFC9000 GTC VSC-12365 camera with HC PL FLUOTAR 10×/0.32 DRY objective. The fluorescence emission was detected at 550 nm upon excitation at 475 nm. Images were processed with Leica Application Suite X (LAS X).

Cell Culture: A549 human wild-type cells, a human alveolar basal epithelial carcinoma cell line (obtained from Abcam), were cultivated in DMEM supplemented with 10% heat-inactivated (30 min at 56 °C) FBS, 1% MEM non-essential amino acid solution as well as 1% penicillin (10 000 U per mL) and 1% streptomycin (10 000 µg mL^{-1}) at 37 °C under a humidified atmosphere with 5% CO_2. Chinese Hamster Ovary (CHO) type cells, an epithelial cell line derived from hamster ovaries was cultivated in F-12K Nut Mix supplemented with 10% heat-inactivated (30 min at 56 °C) FBS, 1% penicillin (10 000 U per mL), and 1% streptomycin (10 000 µg per mL). The RAW-Dual reporter cell line (264.7) was purchased from InvivoGen (San Diego, CA, USA) and cultured in DMEM-GlutaMAXTM medium, which was supplemented with 10% fetal bovine serum, 1% penicillin/streptomycin, 0.02% normocin, and 0.01% zeocin at 37 °C with 5% CO2 saturation. Cells were reseeded at least twice weekly. For splitting of A549 and CHO cells, the cells were washed with DPBS, trypsinated, and resuspended in supplemented culture medium. Splitting of Raw-Dual cells was conducted by scratching cells and resuspending in supplemented culture medium.

For the cell patterning, A549 and CHO cells were washed with PBS, trypsinated, centrifuged (4 min, RT, 500 rpm), and resuspended in supplemented medium, and the Raw-Dual cells were scratched, centrifuged (4 min, RT, 500 rpm), and resuspended prior to seeding on the respective surfaces with a density of 5×10^4 cells per petri dish (8 cm diameter) in 16 mL medium. This was followed by overnight (15 h) incubation in the respective supplemented culture medium at 37 °C under a humidified atmosphere with 5% CO_2. The cells were then treated with calcein-AM staining. To this end, the cells were washed three times with PBS. The cell-culture medium was then replaced by 15–16 mL supplemented medium containing 1 µM calcein-AM solution (prepared from 10 mg mL^{-1} solution in DMSO) and the cells were incubated at 37 °C under a humidified atmosphere with 5% CO_2 for 30 min. Live imaging was performed subsequently on a Leica Thunder DMI8 microscope coupled to a Leica DFC9000 GTC VSC-12365 camera with a N PLAN 5×/0.12 DRY objective. The fluorescence emission was detected using a 519 nm filter upon excitation at 475 nm. Images were processed with Leica Application Suite X (LAS X). All cell-culture experiments were repeated at least in triplicates.

Supporting Information

Supporting Information is available from the Wiley Online Library or from the author.

Acknowledgements

K.K. and A.M.E. contributed equally to this work. The authors thank Uwe Rietzler, Qi Lu for his experimental support, Pierpaolo Moscariello for his comments, and Judith Stickdorn and Alina Heck for cell culture donation and advice. Support by the IMB Microscopy Core Facility is gratefully acknowledged. This study was funded by the Deutsche Forschungsgemeinschaft (DFG, German Research Foundation)—Projektnummer 316249678—SFB 1279 (A05, C01) and Projektnummer 441734479, the Federal Ministry of Education and Research of Germany (BMBF) in the framework of ProMatLeben Polymere InGel-NxG (FKZ: 13XP5086F) as well as Kosmogel (FKZ: 13XP5148). T.M. acknowledges the Foundation for Polish Science financed by the European Union under the European Regional Development Fund (POIR.04.04.00-00-3ED8/17). This work was supported by the Max Planck Graduate Center with the Johannes Gutenberg-Universität Mainz (MPGC).

Open Access funding enabled and organized by Projekt DEAL.

Conflict of Interest

The authors declare no conflict of interest.

Data Availability Statement

The data that support the findings of this study are available in the Supporting Information of this article.

Keywords

amyloid degradation, controlled cell attachment, patterning, self-assembling peptide nanofibers, stimuli-responsive biomaterials

Received: July 19, 2022
Revised: October 14, 2022
Published online: November 10, 2022

[1] T. Aida, E. W. Meijer, S. I. Stupp, *Science* **2012**, *335*, 813.
[2] Y. Li, Y. Xiao, C. Liu, *Chem. Rev.* **2017**, *117*, 4376.
[3] J. d'Alessandro, A. Barbier–Chebbah, V. Cellerin, O. Benichou, R. M. Mège, R. Voituriez, B. Ladoux, *Nat. Commun.* **2021**, *12*, 4118.
[4] D. B. Brückner, N. Arlt, A. Fink, P. Ronceray, J. O. Rädler, C. P. Broedersz, *Proc. Natl. Acad. Sci. U. S. A.* **2021**, *118*, e2016602118.
[5] P. Premnath, A. Tavangar, B. Tan, K. Venkatakrishnan, *Exp. Cell Res.* **2015**, *337*, 44.
[6] M. Ventre, C. F. Natale, C. Rianna, P. A. Netti, *J. R. Soc., Interface* **2014**, *11*, 20140687.
[7] C. M. Kelleher, J. P. Vacanti, *J. R. Soc., Interface* **2010**, *7*, S717.
[8] Y. Lin, M. M. Mazo, S. C. Skaalure, M. R. Thomas, S. R. Schultz, M. M. Stevens, *Chem. Sci.* **2019**, *10*, 1158.
[9] C. T. Mierke, *Front. Phys.* **2021**, *9*, 619.
[10] E. C. Wu, S. Zhang, C. A. E. Hauser, *Adv. Funct. Mater.* **2012**, *22*, 456.
[11] S. Sur, J. B. Matson, M. J. Webber, C. J. Newcomb, S. I. Stupp, *ACS Nano* **2012**, *6*, 10776.
[12] I. Wheeldon, A. Farhadi, A. G. Bick, E. Jabbari, A. Khademhosseini, *Nanotechnology* **2011**, *22*, 212001.
[13] G. Ye, F. Bao, X. Zhang, Z. Song, Y. Liao, Y. Fei, V. Bunpetch, B. C. Heng, W. Shen, H. Liu, J. Zhou, H. Ouyang, *Nanomedicine* **2020**, *15*, 1995.
[14] J. Adamcik, F. S. Ruggeri, J. T. Berryman, A. Zhang, T. P. J. Knowles, R. Mezzenga, *Adv. Sci.* **2021**, *8*, 2002182.
[15] G. G. Glenner, C. W. Wong, *Biochem. Biophys. Res. Commun.* **1984**, *122*, 1131.
[16] A. V. Maltsev, S. Bystryak, O. V. Galzitskaya, *Ageing Res. Rev.* **2011**, *10*, 440.
[17] I. Cherny, E. Gazit, *Angew. Chem., Int. Ed.* **2008**, *47*, 4062.
[18] V. A. Iconomidou, G. Vriend, S. J. Hamodrakas, *FEBS Lett.* **2000**, *479*, 141.
[19] J. E. Podrabsky, J. F. Carpenter, S. C. Hand, *Am. J. Physiol.: Regul., Integr. Comp. Physiol.* **2001**, *280*, R123.
[20] D. Romero, C. Aguilar, R. Losick, R. Kolter, *Proc. Natl. Acad. Sci. U. S. A.* **2010**, *107*, 2230.
[21] A. Taglialegna, I. Lasa, J. Valle, *J. Bacteriol.* **2016**, *198*, 2579.
[22] S. K. Maji, M. H. Perrin, M. R. Sawaya, S. Jessberger, K. Vadodaria, R. A. Rissman, P. S. Singru, K. P. R. Nilsson, R. Simon, D. Schubert, D. Eisenberg, J. Rivier, P. Sawchenko, W. Vale, R. Riek, *Science* **2009**, *325*, 328.
[23] B. Watt, G. van Niel, G. Raposo, M. S. Marks, *Pigment Cell Melanoma Res.* **2013**, *26*, 300.
[24] K. Sato, M. P. Hendricks, L. C. Palmer, S. I. Stupp, *Chem. Soc. Rev.* **2018**, *47*, 7539.
[25] A. K. Das, P. K. Gavel, *Soft Matter* **2020**, *16*, 10065.
[26] N. P. Reynolds, *Biointerphases* **2019**, *14*, 040801.
[27] E. Chuang, A. M. Hori, C. D. Hesketh, J. Shorter, *J. Cell Sci.* **2018**, *131*, jcs189928.
[28] T. Lee, S. Yoo, K. Lee, L. Hwang, Ryou, *Int. J. Mol. Sci.* **2019**, *20*, 5850.
[29] N. Balasco, C. Diaferia, G. Morelli, L. Vitagliano, A. Accardo, *Front. Bioeng. Biotechnol.* **2021**, *9*, 130.
[30] M. Jackson, E. Hewitt, *Biomolecules* **2017**, *7*, 71.
[31] N. Nespovitaya, J. Gath, K. Barylyuk, C. Seuring, B. H. Meier, R. Riek, *J. Am. Chem. Soc.* **2016**, *138*, 846.
[32] G. Son, B. Il Lee, Y. J. Chung, C. B. Park, *Acta Biomater.* **2018**, *67*, 147.
[33] K. Siposova, V. I. Petrenko, O. I. Ivankov, A. Musatov, L. A. Bulavin, M. V. Avdeev, O. A. Kyzyma, *ACS Appl. Mater. Interfaces* **2020**, *12*, 32410.
[34] S. Jordens, J. Adamcik, I. Amar-Yuli, R. Mezzenga, *Biomacromolecules* **2011**, *12*, 187.
[35] S. Xiang, J. Wagner, T. Lückerath, K. Müllen, D. Y. W. Ng, J. Hedrich, T. Weil, *Adv. Healthcare Mater.* **2022**, *11*, 2101854.
[36] P. A. Rühs, J. Adamcik, S. Bolisetty, A. Sánchez-Ferrer, R. Mezzenga, *Soft Matter* **2011**, *7*, 3571.
[37] D. Lin, J. Lei, S. Li, X. Zhou, G. Wei, X. Yang, *J. Phys. Chem. B* **2020**, *124*, 3459.

[38] P. Arosio, T. C. T. Michaels, S. Linse, C. Månsson, C. Emanuelsson, J. Presto, J. Johansson, M. Vendruscolo, C. M. Dobson, T. P. J. Knowles, *Nat. Commun.* **2016**, *7*, 10948.
[39] A. Franco, P. Gracia, A. Colom, J. D. Camino, J. Á. Fernández-Higuero, N. Orozco, A. Dulebo, L. Saiz, N. Cremades, J. M. G. Vilar, A. Prado, A. Muga, *Proc. Natl. Acad. Sci. U. S. A.* **2021**, *118*, e2105548118.
[40] S. Chagri, D. Y. W. Ng, T. Weil, *Nat. Rev. Chem.* **2022**, *6*, 320.
[41] V. Peddie, A. D. Abell, *J. Photochem. Photobiol., C* **2019**, *40*, 1.
[42] A. A. Deeg, T. E. Schrader, S. Kempter, J. Pfizer, L. Moroder, W. Zinth, *ChemPhysChem* **2011**, *12*, 559.
[43] K. Nakamura, W. Tanaka, K. Sada, R. Kubota, T. Aoyama, K. Urayama, I. Hamachi, *J. Am. Chem. Soc.* **2021**, *143*, 19532.
[44] M. Pieszka, A. M. Sobota, J. Gačanin, T. Weil, D. Y. W. Ng, *ChemBioChem* **2019**, *20*, 1376.
[45] J. Gačanin, J. Hedrich, S. Sieste, G. Glaßer, I. Lieberwirth, C. Schilling, S. Fischer, H. Barth, B. Knöll, C. V. Synatschke, T. Weil, *Adv. Mater.* **2019**, *31*, 1805044.
[46] Y. Luo, M. S. Shoichet, *Nat. Mater.* **2004**, *3*, 249.
[47] T. Matsuda, T. Sugawara, *J. Biomed. Mater. Res.* **1995**, *29*, 749.
[48] D. Ryan, B. A. Parviz, V. Linder, V. Semetey, S. K. Sia, J. Su, M. Mrksich, G. M. Whitesides, *Langmuir* **2004**, *20*, 9080.
[49] S. Zhang, L. Yan, M. Altman, M. Lässle, H. Nugent, F. Frankel, D. A. Lauffenburger, G. M. Whitesides, A. Rich, *Biomaterials* **1999**, *20*, 1213.
[50] F. M. Yavitt, B. E. Kirkpatrick, M. R. Blatchley, K. S. Anseth, *Biomater. Sci. Eng.* **2022**, acsbiomaterials.1c01450.
[51] C. A. DeForest, K. S. Anseth, *Angew. Chem., Int. Ed.* **2012**, *51*, 1816.
[52] R. J. Wade, E. J. Bassin, W. M. Gramlich, J. A. Burdick, *Adv. Mater.* **2015**, *27*, 1356.
[53] D. S. Hernandez, E. T. Ritschdorff, S. K. Seidlits, C. E. Schmidt, J. B. Shear, *J. Mater. Chem. B* **2016**, *4*, 1818.
[54] I. Batalov, K. R. Stevens, C. A. DeForest, *Proc. Natl. Acad. Sci. U. S. A.* **2021**, *118*, e2014194118.
[55] B. D. Fairbanks, S. P. Singh, C. N. Bowman, K. S. Anseth, *Macromolecules* **2011**, *44*, 2444.
[56] C. Yang, F. W. DelRio, H. Ma, A. R. Killaars, L. P. Basta, K. A. Kyburz, K. S. Anseth, *Proc. Natl. Acad. Sci. U. S. A.* **2016**, *113*, E4439.
[57] A. M. Kloxin, A. M. Kasko, C. N. Salinas, K. S. Anseth, *Science* **2009**, *324*, 59.
[58] J. B. Matson, Y. Navon, R. Bitton, S. I. Stupp, *ACS Macro Lett.* **2015**, *4*, 43.
[59] S. V. Wegner, O. I. Sentürk, J. P. Spatz, *Sci. Rep.* **2016**, *5*, 18309.
[60] A. M. Ender, K. Kaygisiz, H.-J. Räder, F. J. Mayer, C. V. Synatschke, T. Weil, *ACS Biomater. Sci. Eng.* **2021**, *7*, 4798.
[61] C. Schilling, T. Mack, S. Lickfett, S. Sieste, F. S. Ruggeri, T. Sneideris, A. Dutta, T. Bereau, R. Naraghi, D. Sinske, T. P. J. Knowles, C. V. Synatschke, T. Weil, B. Knöll, *Adv. Funct. Mater.* **2019**, *29*, 1809112.
[62] M. E. Lee, E. Gungor, A. M. Armani, *Macromolecules* **2015**, *48*, 8746.
[63] S. Sieste, T. Mack, E. Lump, M. Hayn, D. Schütz, A. Röcker, C. Meier, K. Kaygisiz, F. Kirchhoff, T. P. J. Knowles, F. S. Ruggeri, C. V. Synatschke, J. Münch, T. Weil, *Adv. Funct. Mater.* **2021**, *31*, 2009382.
[64] N. J. Greenfield, *Nat. Protoc.* **2007**, *1*, 2876.
[65] A. Adochitei, G. Drochioiu, *Rev. Roum. Chim.* **2011**, *56*, 783.
[66] M. Jackson, H. H. Mantsch, *Crit. Rev. Biochem. Mol. Biol.* **1995**, *30*, 95.
[67] C. Xue, T. Y. Lin, D. Chang, Z. Guo, *R. Soc. Open Sci.* **2017**, *4*, 160696.
[68] J. Jeong, Y. Lee, Y. Yoo, M. K. Lee, *Colloids Surf., B* **2018**, *162*, 306.
[69] W. Y. Seow, K. Kandasamy, G. S. L. Peh, J. S. Mehta, W. Sun, *ACS Biomater. Sci. Eng.* **2019**, *5*, 4067.
[70] F. Topuz, A. Nadernezhad, O. S. Caliskan, Y. Z. Menceloglu, B. Koc, *Carbohydr. Polym.* **2018**, *201*, 105.
[71] R. Armisen, *Hydrobiologia* **1991**, *221*, 157.
[72] S. Arnott, A. Fulmer, W. E. Scott, I. C. M. Dea, R. Moorhouse, D. A. Rees, *J. Mol. Biol.* **1974**, *90*, 269.
[73] K. Nakamura, R. Kubota, I. Hamachi, *ChemRxiv* **2022**, 10.26434/chemrxiv
[74] A. A. Patil, C.-K. Chiang, C.-H. Wen, W.-P. Peng, *Anal. Chim. Acta* **2018**, *1031*, 128.
[75] X. Zhan, D. M. Desiderio, *Int. J. Mass Spectrom.* **2009**, *287*, 77.